Characterization of Crystalline CsPbBr₃ Perovksite Dosimeters for Clinical Radiotherapy

Mara Bruzzi[1,2]* and Cinzia Talamonti[2,3]

[1]Dipartimento di Fisica e Astronomia, Università degli Studi di Firenze, Firenze, Italy, [2]Istituto Nazionale di Fisica Nucleare, Sezione di Firenze, Firenze, Italy, [3]Dipartimento di Scienze Biomediche Sperimentali e Cliniche "Mario Serio" Università degli Studi di Firenze, Firenze, Italy

Lead halide perovskite $CsPbBr_3$ is a wide-gap semiconductor material potentially very attractive for next generations of real-time monitors and particle detectors in high-energy physics. Here, we present the first characterization of crystalline $CsPbBr_3$ point dosimeters with submillimeter size, under 6 MV X-photon beams used in clinical radiotherapy. Current response of the devices proved to be promising in terms of fast rise and decay times, of the same order of the X-ray beam onset and offset ones; absence of polarization effects; reproducibility to repeated irradiations; and linearity of the collected charge as a function of the absorbed dose. Comparing the measured sensitivity with the theoretical one, a charge collection distance of about 100 μm has been evaluated, of the same order of the linear dimensions of crystallites within the samples, suggesting that recombination centers are mainly placed at grain boundaries. A much higher sensitivity per unit area measured with crystalline $CsPbBr_3$ as compared with drop-casted ones can be explained in terms of a less disordered crystalline structure. This work opens the way to $CsPbBr_3$ point dosimeters, with linear dimensions meeting the strict spatial resolution constraints for bidimensional dose mapping required in clinical radiotherapy.

INTRODUCTION

The ever increasing interest for novel devices in medical applications has recently focused toward perovskite-based semiconductors. In particular, lead halide perovskites, with crystal structure $APbX_3$ ($A = Cs^+$, $CH_3NH_3^+$ methylammonium, $CH(NH_2)^{2+}$), are potentially quite attractive for future photodetectors and dosimeters in advanced medical imaging and clinical radiotherapy [1–7]. In these latter applications, high-energy X-Ray beams focused on tumors are required to spare as much as possible the surrounding healthy tissues. This requirement is fulfilled by most recent technology now used in hospital, volumetric modulated arc therapy (VMAT), where the delivered dose conformation to the tumor volume is obtained by continuously changing spatial distribution of multi-linear collimator (MLC) leaves, dose rates, and gantry rotation speed [8]. In such irradiation conditions, devices used to measure 2D and 3D dose maps are subjected to severe constraints as high resolutions in time and space, ability to cover nonplanar geometries with flexible substrates, and use in transmission mode for *in vivo* verifications. The bidimensional maps of dose are typically obtained using arrays and matrices of pixels, and the spatial resolution of the device is determined by both pixel dimensions and pitch. The principle of operation of a real-time dosimeter is to collect charge at electrodes when the active volume is subjected to a flux of high-energy particles. Linear behavior is a

FIGURE 1 | Mean energy value required to create an e–h pair in several semiconductor materials. The two solid lines evidence the range of applicability of the Klein's empirical rules. The halide perovksite under study in this work is part of a group of materials not following this rule.

stringent requirement of the device: the collected charge must be directly proportional to the absorbed dose. The sensitivity of the device is defined as the slope of the charge vs dose curve, $S = \frac{Q}{D}$, with D being the absorbed dose and Q the charge collected at the electrode. The sensitivity per unit volume of a semiconductor, $S_V = \frac{S}{Volume}$, can be calculated (D_r, dose rate; q, electronic charge) as [9]:

$$S_V = \frac{qG}{D_r} = \frac{q\rho}{E_i}, \tag{1}$$

where G is the e-h pair generation rate:

$$G = \frac{D_r\rho}{E_i}, \tag{2}$$

where ρ is the mass density and E_i is the mean ionization energy. This latter is the average energy needed to create one electron–hole (e-h) pair. It is usually determined by the Klein's semiempirical relationship [10]:

$$E_i = \frac{14}{5}E_g + r(\hbar\omega_r). \tag{3}$$

Here, $r(\hbar\omega_r)$ is the optical phonon loss term, usually in the range $0.5 eV - 1.0 eV$. The Klein's model proceeds on the premises that the average amount of radiation energy consumed per pair can be accounted for by a sum of three contributions: intrinsic bandgap

(E_g), optical phonon losses, and residual kinetic energy; the latter is calculated as $\frac{9}{5}E_g$.

The material proposed in this study, a lead halide perovskite, $CsPbBr_3$, is a semiconductor with an exceptionally high theoretical sensitivity. Using Klein's relationship, the mean ionization energy of $CsPbBr_3$, characterized by an energy gap E_g = 2.4 eV at 300 K, should lie in the range: E_i = 7.2–7.7 eV. Nonetheless, recent results on $CsPbBr_3$ single crystals for high-resolution gamma detectors allowed for the experimental determination of a significantly lower mean ionization value, E_i = 5.3 eV [11]. Of note is that E_i mean ionization energies smaller than those predicted by the Klein's relationship are observed also in other halide semiconductors, such as HgI_2, TlBr, and PbI_2 [12]. **Figure 1** resumes the mean energy E_i as a function of the energy gap for several semiconductors, evidencing those following the Klein's rules and those lying outside its semiempirical prediction. Values have been taken from the literature [10–13]. In the plot, two solid lines in black are indicating the range of linear dependence of Klein's formula in case $0.5eV < r(\hbar\omega_r) < 1.0 eV$. Blue dots are indicating those semiconductors following the Klein's rule, and red squares show semiconductors not following it (red line is a guide-eye line). $CsPbBr_3$ lies within this second class of materials.

The relatively high mass density, 4.55 g/cm^3 combined with the low mean ionization energy, results in a sensitivity per unit volume for $CsPbBr_3$, $S_V = \frac{q\rho}{E_i}$ = 860nC/(Gy · mm^3), definitely higher than those, for example, of silicon and diamond, respectively, 637nC/Gymm^3 and 217nC/(Gy · mm^3), the two materials now most widely used as on-line dosimeters [9].

Further, other arguments in favor of using $CsPbBr_3$ in real-time radiation monitoring applications are as follows:

$CsPbBr_3$ is characterized by easy deposition methods, allowing to deposit on almost any kind of substrates nanostructures, single crystals and polycrystalline thin films [14];

the material is potentially defect tolerant and less prone to mid-gap states as conventional semiconductors such as Si, GaAs, and InP, since main defects in $CsPbBr_3$ are mostly related to shallow and intra-band levels [15];

besides promising transport properties as high diffusion lengths and high charge carrier mobilities [16], $CsPbBr_3$ has a relatively high bandgap so that it can be considered intrinsically "radiation resistant" as a particle detector. In fact, defect-assisted thermal generation of electron–hole pairs, usually originating noise in a radiation detector, should be in principle negligible at room temperature, even after very high accumulated doses [17].

This work reports on first characterizations of crystalline $CsPbBr_3$ as dosimeters for clinical radiotherapy. In-house manufactured devices have been tested under 6 MV X-ray beams with dose and dose rates in the range of typical interest for clinical applications, in view to test the feasibility of high spatial resolution point dosimeters which could be used as pixel elements in linear and bidimensional arrays. Point dosimeters with 0.4 mm linear size have been manufactured to achieve spatial resolutions in bidimensional mapping below 1 mm.
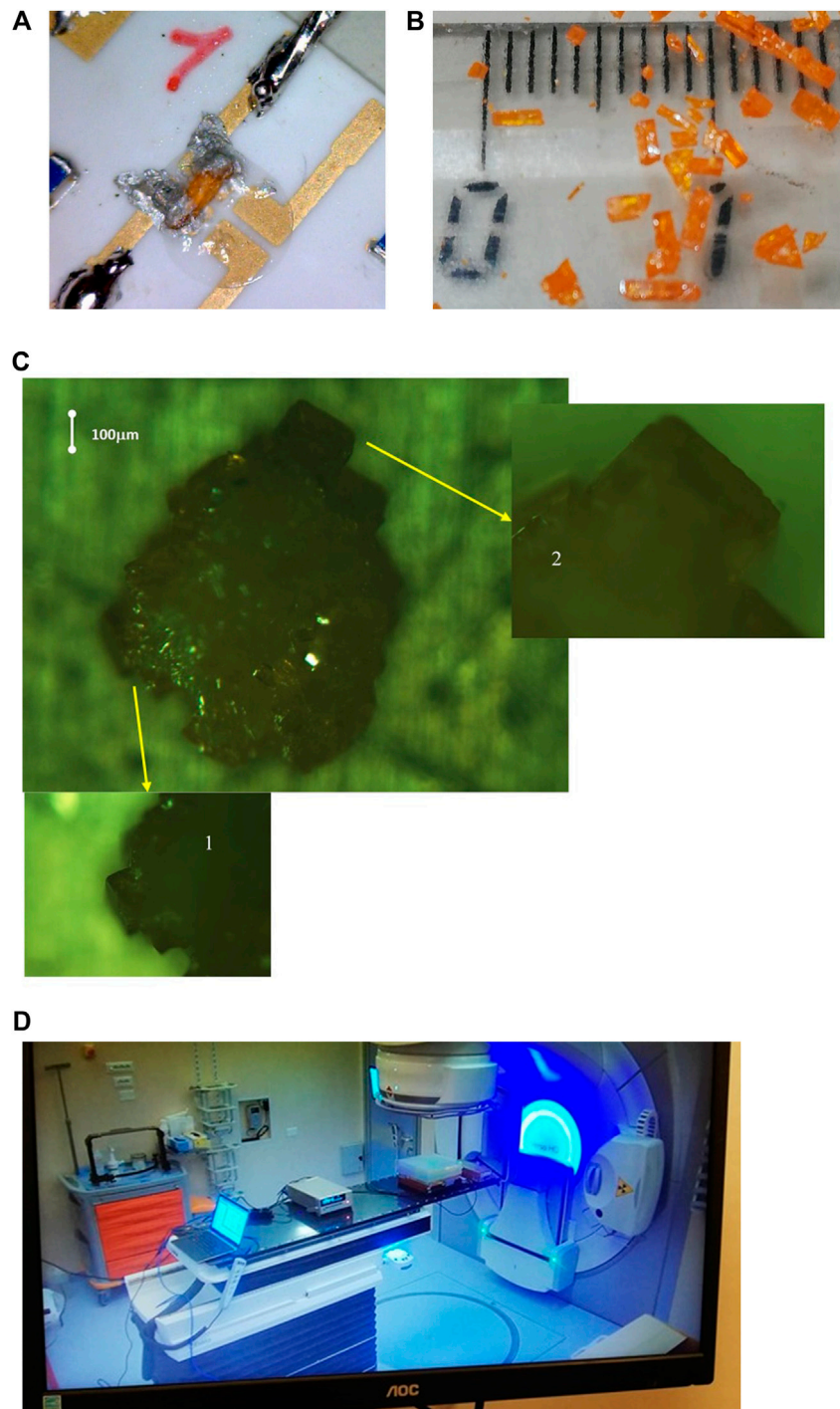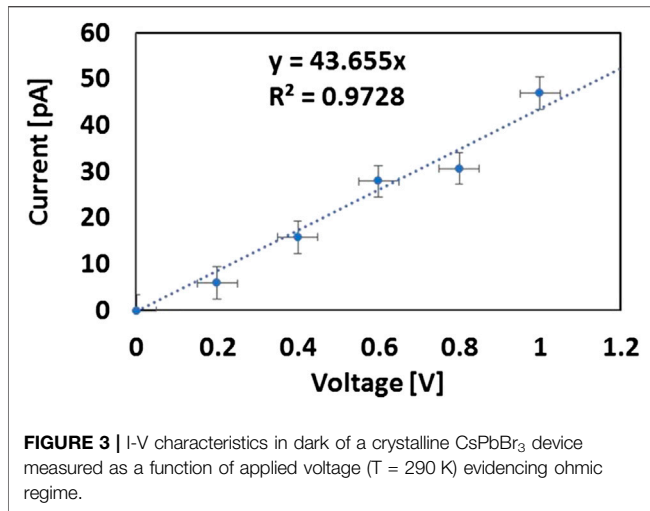
FIGURE 2 | (A) A crystalline CsPbBr3 sample mounted on the alumina PCB equipped with Au contacts. **(B)** Photograph of the set of millimeter-sized crystalline CsPbBr3 samples used in this study; **(C)** Optical microscope photographs evidencing the polycrystalline structure of our samples. Crystallites with dimensions up to about 100 μm linear size are visible in insets 1 and 2; **(D)** The perovskite dosimetric system running under the X-ray beam within the treatment room at Dipartimento di Scienze Biomediche Sperimentali e Cliniche "Mario Serio," Universitá di Firenze, Italy.

Linearity of response with the absorbed dose and the dosimetric sensitivity is evaluated. Active volume and sensitivity per unit surface are then compared with those obtained in previous works using similar samples produced as drop-casted films.

EXPERIMENTAL PROCEDURE

Crystalline CsPbBr$_3$ samples have been grown using a solvent/anti-solvent procedure, starting from a saturated solution of the

FIGURE 3 | I-V characteristics in dark of a crystalline CsPbBr$_3$ device measured as a function of applied voltage (T = 290 K) evidencing ohmic regime.

CsBr and PbBr$_2$ 1:1 molar ratio in dimethyl sulfoxide. Details on the growth method are given in [18, 19]. **Figure 2B** shows the set of millimeter-sized crystalline CsPbBr$_3$ samples used in this study. Optical microscope photographs evidencing the polycrystalline structure of the samples, composed by crystallites with different orientations and variable dimensions, up to about 200 μm linear size, are shown in **Figure 2C**. More details on the crystalline quality of the samples are reported elsewhere [18]. Details on a full sample characterization by scanning electron microscope (SEM), X-ray diffraction (XRD), and photoluminescence (PL) spectroscopy under continuous wave and picosecond excitation in the temperature range 10–300 K to assess the quality of the material can be found in Ref. [20].

To produce point dosimeters, crystalline grains have been glued with silver paint in between Au planar contacts deposited on alumina printed circuit boards (PCBs). Electrode distance is 0.4 mm, and crystal surface area normal to the beam is about 0.16 mm^2. The crystalline sample mounted on the PCB is then covered with PolyMethylMethAcrylate (PMMA) to prevent deterioration due to air and water vapor exposure [20]. **Figure 2A** shows a photograph of a crystalline sample mounted on an alumina PCB equipped with Au contacts, covered with PMMA [21].
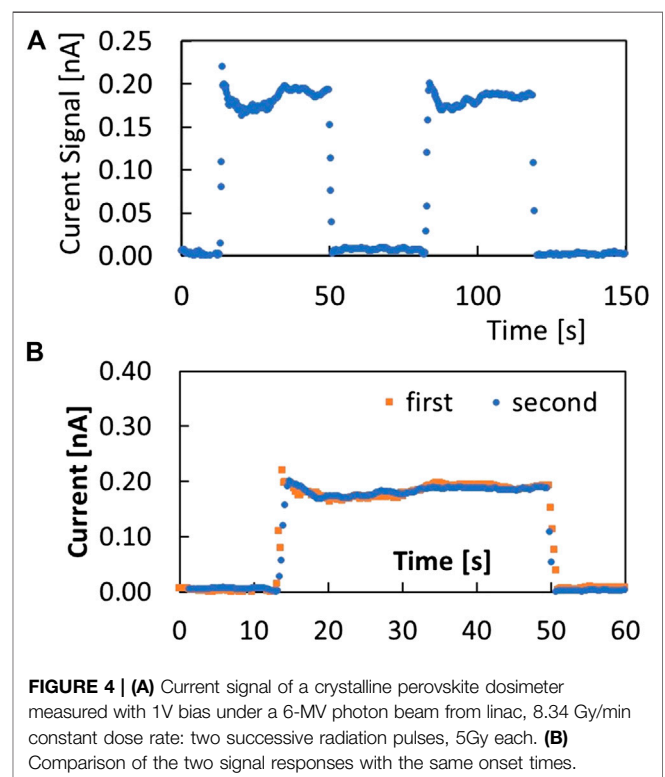
To perform the dosimetric characterization, the device is placed within a PMMA finger inserted into a solid water phantom, positioned under the linac head at 100 cm from the source, kept under 10 cm depth of water equivalent phantom (PMMA, solid water) in view to achieve charge particle equilibrium conditions. The beam size is 10 cm x 10 cm to provide field uniformity without penumbra effects on the device which is placed on the central axis. The device is connected to a Keithley 6517A for current readout and voltage source supply remotely driven during irradiation by PC with MATLAB software. Electron read-out integrating times are in the range 10–40 ms. **Figure 2D** shows the device ready for dosimetric tests within the treatment room at Radiotherapy Section of

Dipartimento di Scienze Biomediche Sperimentali e Cliniche "Mario Serio," Università di Firenze, Italy.

Prior irradiation, we measured the dark current–voltage (IV) characteristics of the device mounted in the finger. After applying an external voltage across the electrodes, we waited a few minutes to achieve current stabilization [22, 23]. We used voltages in the range of ±1 V, to keep a sufficiently low electric field within the material. In fact, recent studies on CsPbBr$_3$ samples [23] showed that, if a high electric field is applied to crystals, defect proliferation phenomena, originating from ion migration, may take place. The resulting IV characteristics are shown in **Figure 3**. Within our measurement errors, evaluated, respectively, ±3 pA and ±50 mV in these operative conditions, data can be interpreted considering an ohmic regime, with room temperature resistivity of about 0.8 GΩcm.

EXPERIMENTAL RESULTS AND DISCUSSION

To calibrate our crystalline perovskite dosimeters, charge and current signals have been measured under conventional 6 MV X-photon beams from a linac, in a uniform 10 × 10 cm^2 radiation field. The device is kept at room temperature, and a constant voltage of 1V has been applied across electrodes. To favor current stabilization, we started each measurement a few minutes after bias application. A first irradiation cycle is performed in order to "prime" the device, namely, to let traps present in the material to capture charges and then to passivate [18]. In general, a dose of about 1–3 Gy is required, depending on the samples. Then, the
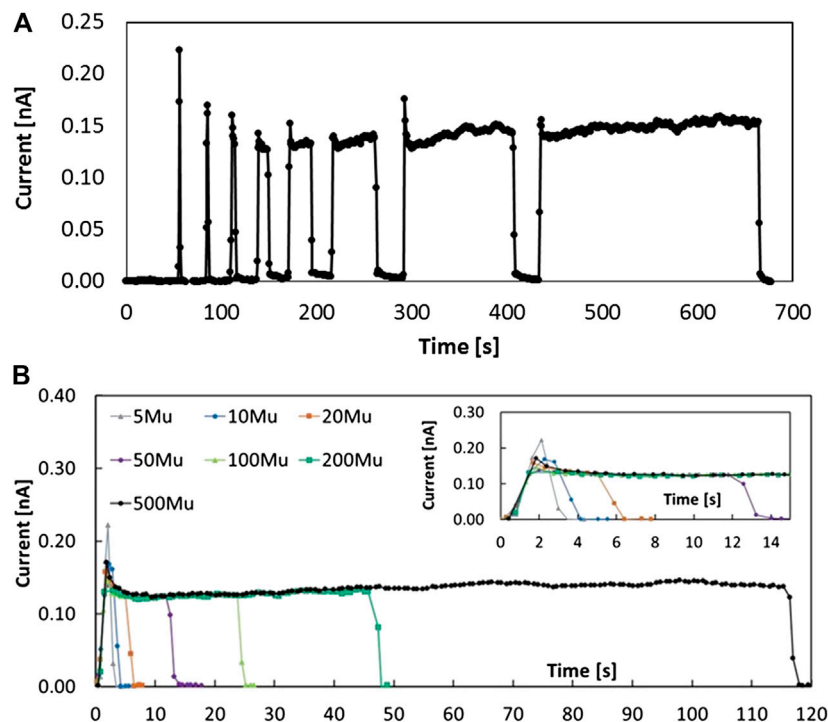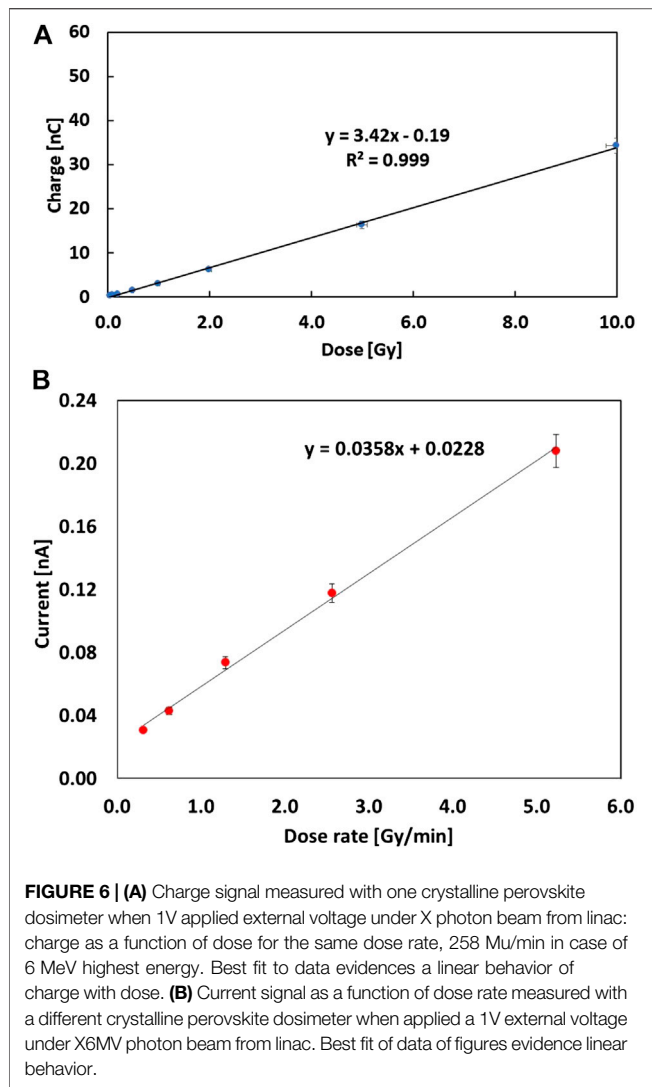

FIGURE 4 | **(A)** Current signal of a crystalline perovskite dosimeter measured with 1V bias under a 6-MV photon beam from linac, 8.34 Gy/min constant dose rate: two successive radiation pulses, 5Gy each. **(B)** Comparison of the two signal responses with the same onset times.

FIGURE 5 | Dosimetric test results of a crystalline perovskite dosimeter under linac 6 MV X-photon beam irradiation at the same dose rate, 2.58 Mu/min, when 1V external voltage is applied across the sample. **(A)** Current signal as a function of time for seven successive pulses and increasing duration; **(B)** comparison of current signals with the same onset times for different doses, in the range up to 500Mu. Inset highlights the shorter pulses.

current signal, background subtracted, appears to be reproducible when using the same doses and dose rates. As an example, in **Figure 4A**, we show the current signal measured when two successive radiation pulses, each corresponding to a dose of 500cGy, are delivered under a constant dose rate (8.34 Gy/min). The current signal measured when the beam is switched on is quite similar for the two radiation pulses. In fact, current signals appear to be reproducible, as evidenced by the plot of **Figure 4B**, where the two signals are aligned with the same onset times. Moreover, current signals are characterized by fast decay and rise times, of the order of 1s, with the absence of transients due to polarization effects or persistent currents. The linac pulse repetition frequencies (PRF) are in the range 50–400 Hz and our read-out electronics is integrating the signal on a time frame of 10 ms, measuring the current signal under about a 4-Hz rate. In these conditions, we are not actually able to evaluate the slew rate of the sensor (in future, we plan to refine our timing measurements by means of a *trans*-impedance front end).

The dosimetric response as a function of the dose has been studied measuring the current signal of our devices under an X-ray beam with a constant dose rate and increasing exposure times, to cover a dose range from 5cGy to 10Gy. **Figure 5A** shows the current signal (after background subtraction) measured with one CsPbBr$_3$ device during a cycle of seven successive 6 MV photon beam irradiation pulses with D_r = 2.58 Gy/min. The complex structure of the signal for different time elongations is evidenced in **Figure 5B**, where pulses corresponding to

different doses have been aligned in order to have the same onset times. Current instability observed in **Figures 4**, **5** is probably due to priming of defects which are capturing/releasing defects, activating especially at the early stage of each irradiation step. Anyway, the plot highlights how all current signals follow the same pattern, developing with the same function with time when increasing the pulse duration. Concerning the measured rise and decay times, they can be considered fast, when using conventional beams where relevant delivery times are of the order or higher than 1s.

The charge response at different doses is measured as the integral of the current response during each irradiation pulse, after subtraction of the extrapolated background current. The plot of the collected charge as a function of the dose is shown in **Figure 6A**. Results evidence the linear dependence of the collected charge on the absorbed dose. We observe that the current instability measured during irradiation is not influencing the dose calculated by current signal integration at each delivery step. This can be explained considering that active defects are capturing and releasing charged carriers within the time window of the dose delivery itself; thus, they are not affecting the dose calculation. To determine the sensitivity of our device, data have been best-fitted to a line: slope value is S = 3.4 nC/Gy. To be able to work with modern radiotherapy machines, as VMAT, where dose rates are continuously varying during treatments, a dosimetric device should be characterized also by a linear dependence of the current signal on the dose rate. The

FIGURE 6 | (A) Charge signal measured with one crystalline perovskite dosimeter when 1V applied external voltage under X photon beam from linac: charge as a function of dose for the same dose rate, 258 Mu/min in case of 6 MeV highest energy. Best fit to data evidences a linear behavior of charge with dose. **(B)** Current signal as a function of dose rate measured with a different crystalline perovskite dosimeter when applied a 1V external voltage under X6MV photon beam from linac. Best fit of data of figures evidence linear behavior.

current signal measured with another device (same material, and same voltage applied and contact geometry) under four different dose rates in the range 30–530 Mu/min (X6MV photon beam) is plotted as a function of the dose rate in **Figure 6B**.

From the sensitivity S value determined by our charge vs dose measurements, it is possible to get a first evaluation of the charge collection distance, *ccd*, namely, the average distance the e–h pairs created by radiation can travel in our samples before they are recombined at a defect. Starting from the known theoretical value of the sensitivity per unit volume, $S_V = 860$ nC/(Gy mm^3), considering our sample as a cube with size 0.4 mm, we estimate: $ccd = \sqrt[3]{\frac{S}{S_V}} \sim 100 \mu m$. We note that this value is in agreement with estimations made by optical microscopy of the linear dimension of the biggest grains present within our crystalline CsPbBr$_3$ samples (see **Figure 2B**). According to this observation, the deficit in charge collection should be mainly attributed to defects at grain boundaries, acting as non-radiative recombination channels responsible for the annihilation of e–h pairs. As a consequence of this deficit in charge collection, the

sensitivity per unit volume of our device is about 50 nC/(Gy mm^3), lower of the one calculated for diamond 217 nC/(Gymm^3).

Finally, we observe that first results obtained with crystalline CsPbBr$_3$ dosimeters compare favorably with those previously obtained with drop-casted CsPbBr$_3$ thin films deposited on similar PCBs [6]. This holds in particular for the sensitivity per unit surface for crystalline devices, about 22 nC/(Gy mm^2), much higher than 1.4 nC/(Gy mm^2), the value measured with drop-casted CsPbBr$_3$ thin films [6]. As a consequence of this increased sensitivity per unit surface, crystalline CsPbBr$_3$ can act as point dosimeters with linear dimensions well below 1 mm, so matching the ultimate constraint for spatial resolution in bidimensional mapping of the dose in clinical radiotherapy.

CONCLUSION

Lead halide perovskite CsPbBr$_3$ is a wide-gap semiconductor material potentially very attractive for next generations of real-time dosimeters and possibly for future particle detectors in high-energy physics. This work reports on first experimental results concerning crystalline CsPbBr$_3$ samples. First submillimeter point dosimeters have been produced and tested with a high-energy X-photon beam used for clinical radiotherapy applications. First results reported here are promising in terms of fast rise and decay times, absence of polarization effects during irradiation, reproducibility of the current signal in repeated pulses, and linearity of the collected charge as a function of the absorbed dose. If we compare the measured sensitivity with the theoretical one, we estimate a charge collection distance *ccd* of about 100 μm, a value of the same order of the linear dimensions of the crystallites composing the material. This suggests that recombination centers responsible for incomplete charge collection may be placed at grain boundaries. If so, crystalline samples should be less subjected to the detrimental effects due to defects then drop-casted samples, composed by grains of only a few micron size [6, 18]. In order to further increase the sensitivity per unit volume of our devices, in future, a more efficient charge collection should be achieved, for example, by further increasing the linear dimension of the crystallites and their orientation through the sample. This can be, in principle, performed by a detailed control of the growth process parameters [24]; this will be the subject of a forthcoming work.

Finally, we observe that the crystalline samples tested in this work are characterized by a much higher sensitivity per unit area than that of drop-casted CsPbBr$_3$ thin films. This opens the way to CsPbBr$_3$ point dosimeters with linear dimensions below 1mm, well matching the strict spatial resolution constraints in bidimensional dose mapping required in clinical radiotherapy. In future, we plan to perform studies with the same devices under IMRT and VMAT beams. To this purpose, the read-out electronics will be optimized to evaluate correctly even doses delivered with times lower than 1s. Further, we are planning to measure output factors, namely, the response of the device under beams of decreased size, to study the effect of the

profile of a collimated x-ray beam on the dosimetric response of the device.

DATA AVAILABILITY STATEMENT

The raw data supporting the conclusions of this article will be made available by the authors, without undue reservation.

AUTHOR CONTRIBUTIONS

Conceptualization, MB and CT; methodology, MB and CT; software, MB; device manufacturing, MB; validation, MB and CT; formal analysis, MB; investigation, MB and CT; resources, MB and CT; data curation, MB and CT; writing—original draft preparation, MB; writing—review and editing, MB and CT; supervision, MB; project administration, MB; and funding acquisition, MB.

REFERENCES

1. Tsai H, Liu F, Shrestha S, Fernando K, Tretiak S, Scott B, et al. A sensitive and robust thin-film x-ray detector using 2D layered perovskite diodes. *Sci Adv* (2020) 6(15):815. doi:10.1126/sciadv.aay0815

2. Saidaminov MI, Adinolfi V, Comin R, Abdelhady AL, Peng W, Dursun I, et al. Planar-integrated single-crystalline perovskite photodetectors. *Nat Commun* (2015) 6:8724. doi:10.1038/ncomms9724

3. Pierre A, Deckman I, Lechêne PB, Arias AC. High detectivity all-printed organic photodiodes. *Adv Mater* (2015) 27(41):6411–7. doi:10.1002/adma.201502238

4. Kim YC, Kim KH, Son DY, Jeong DN, Seo JY, Choi YS, et al. Printable organometallic perovskite enables large-area, low-dose X-ray imaging. *Nature* (2017) 550(7674):87–91. doi:10.1038/nature24032

5. Gill HS, Elshahat B, Kokil A, Li L, Mosurkal R. Flexible perovskite based X-ray detectors for dose monitoring in medical imaging applications. *Phys Med* (2018) 5:20. doi:10.1016/j.phmed.2018.04.001

6. Bruzzi M, Talamonti C, Calisi N, Caporali S, Vinattieri A. First proof-of-principle of inorganic perovskites clinical radiotherapy dosimeters. *Appl Phys Lett Mat* (2019) 7:051101. doi:10.3390/nano10010060

7. Stoumpos CC, Malliakas CD, Peters JA, Liu Z, Sebastian M, Im MJ, et al. Crystal growth of the perovskite semiconductor CsPbBr3: a new material for high-energy radiation detection. *Cryst Growth Des* (2013) 13 2722–7.

8. Allison RR, Sibata C, Patel R. Future radiation therapy: photons, protons and particles. *Future Oncol* (2013) 9:493–504. doi:10.2217/fon.13.13

9. Bruzzi M. Novel silicon devices for radiation therapy monitoring. *Nucl Instrum Methods Phys Res Sect A* (2016) 809:105. doi:10.1016/j.nima.2015.10.072

10. Klein CA. Bandgap dependence and related features of radiation ionization energies in semiconductors. *J Appl Phys* (1968) 39:2029. doi:10.1063/1.1656484

11. Yihui H, Matei L, Jung HJ, McCall KM, Chen M, Stoumpos CC, et al. High spectral resolution of gamma-rays at room temperature by perovskite CsPbBr3 single crystals. *Nat Commun* (2018) 9:1609. doi:10.1038/s41467-018-04073-3

12. Shah KS, Lund JC, Olschner G, Moy L, Squillante MR. Thallium bromide radiation detectors. *IEEE Trans Nucl Sci* (1989) 36:199–202. doi:10.1109/23.34434

13. Owens A, Peacock A. Compound semiconductor radiation detectors. *Nucl Instrum Methods Phys Res A* (2004) 531:18–37. doi:10.1016/j.nima.2004.05.071

14. Seth S, Samanta A. A facile methodology for engineering the morphology of CsPbX3 perovskite nanocrystals under ambient condition. *Sci Rep* (2016) 6:37693. doi:10.1038/srep37693

15. Kovalenko MV, Protesescu L, Bodnarchuk MI. Properties and potential optoelectronic applications of lead halide perovskite nanocrystals *Science* (2017) 358:745–50. doi:10.1126/science.aam7093

16. Motta C, El-Mellouhi F, Sanvito S. Charge carrier mobility in hybrid halide perovskites. *Sci Rep* (2014) 5:12746. doi:10.1038/srep12746

17. Bruzzi M, Sadrozinski HFW, Seiden A. Comparing radiation tolerant materials and devices for ultra rad-hard tracking detectors. *Nucl Instrum Methods Phys Res A* (2007) 579:754–61. doi:10.1016/j.nima.2007.05.326

18. Bruzzi M, Falsini N, Calisi N, Vinattieri A. Electrically active defects in polycrystalline and single crystal metal halide perovskite. *Energies* (2020) 13:1643. doi:10.3390/en13071643

19. Rakita Y, Kedem N, Gupta S, Sadhanala A, Kalchenko V, Böhm ML, et al. Low-temperature solution-grown CsPbBr3 single crystals and their characterization. *Cryst Growth Des* (2016) 16:5717–25.doi:10.1021/acs.cgd.6b00764

20. Gabelloni F, Biccari F, Falsini N, Calisi N, Caporali S, Vinattieri A. Long-living nonlinear behavior in CsPbBr3 carrier recombination dynamics. *Nanophotonics* (2019) 8:1447–55. doi:10.1515/nanoph-2019-0013

21. Calisi N, Caporali S, Milanesi A, Innocenti M, Salvietti E, Bardi U. Composition-dependent degradation of hybrid and inorganic lead perovskites in ambient conditions. *Top Catal* (2018) 61:1201–8.

22. Chen C, Fu Q, Guo P, Chen H, Wang M, Luo W, et al. Ionic transport characteristics of large-size CsPbBr3 single crystals. *Mater Res Express* (2019) 6:115808. doi:10.1088/2053-1591/ab4d79

23. Zhang BB, Wang F, Zhang H, Xiao B, Sun Q, Guo J, et al. Defect proliferation in CsPbBr3 crystal induced by ion migration. *Appl Phys Lett* (2020) 116:063505. doi:10.1063/1.5134108

24. Dirin DN, Cherniukh I, Yakunin S, Shynkarenko Y, Kovalenko VK. Solution-grown CsPbBr3 perovskite single crystals for photon detection. *Chem Mater* (2016) 28 (23):8470–4. doi:10.1021/acs.chemmater.6b04298